Comparison of ZrB2-SiC, HfB2-SiC and HfB2-SiC-Y2O3 oxidation mechanisms in air using LIF of BO2(g)

V. Guérineau, Gautier Vilmart, Nelly Dorval, Aurélie Julian-Jankowiak

Comparison of ZrB_2-SiC, HfB_2-SiC and HfB_2-SiC-Y_2O_3 oxidation mechanisms in air using LIF of $BO_2(g)$

V. Guérineau[1], G. Vilmart[2], N. Dorval[2] andA. Julian-Jankowiak[1,*]

[a] DMAS, ONERA, Université Paris-Saclay, F-92322 Châtillon, France
[b] DPHY, ONERA, Université Paris-Saclay, F-91123 Palaiseau, France

*Corresponding author: aurelie.jankowiak@onera.fr

vincent1guerineau@gmail.com,   aurelie.jankowiak@onera.fr,   nelly.dorval@onera.fr, gautier.vilmart@onera.fr

Declaration of interest: none

Abstract:

The oxidation behaviour of ZrB_2-SiC, HfB_2-SiC and HfB_2-SiC-Y_2O_3 is studied using the real-time Laser-Induced Fluorescence (LIF) detection of $BO_2(g)$ evaporated from samples heated up to 1873 K in dry air. For each composition, the relevant steps of oxidation (silica formation, volatilization, etc.) can be precisely determined. Moreover, the influence of composition on the oxidation behaviour, and more precisely on the B_2O_3/SiO_2 ratio in the glassy phase, can be understood and described by monitoring the LIF signal from the $BO_2(g)$ radical. Thus, this technique has confirmed the potential of the HfB_2-SiC-Y_2O_3 composition as a Ultra High Temperature Ceramic (UHTC) material.

KEYWORDS: (A) ceramic; (C) high temperature corrosion; (C) oxidation; (B) spectroscopy; (B) Laser Induced Fluorescence

1. Introduction

Ultra-High Temperature Ceramics (UHTC) are extensively investigated as materials for applications in very high temperatures (>2073 K) and oxidising or corrosive atmospheres. Among this material family, UHTC borides, such as ZrB_2 and HfB_2-based ceramics, are particularly interesting since the melting points of these materials are high, and the mechanical, thermal and chemical properties are excellent. Hence, they might be ideal candidates for developing thermal protection systems on hypersonic aerospace vehicles or atmospheric re-entry vehicles which require a good oxidation resistance under severe conditions.

Thus, studying and understanding the oxidation resistance of such materials is essential. The influence of the SiC addition or of other additives (e.g. $TaSi_2$, $MoSi_2$) has been largely studied [1–5] so that, the oxidation behaviour of ZrB_2-SiC and HfB_2-SiC is relatively well known up to 2073 K in air [6–12]. A few studies have also been carried out at higher temperatures and under other atmospheres than air [13–19], for instance in the presence of humidity or in an oxyacetylene flame.

Although the key role of the borosilicate layer [1,20,21] and finally of the ZrO_2 or HfO_2 layer [13,18,22] has been demonstrated, a very few studies attempted the *in situ* investigation of its behaviour during an oxidation test. The thermogravimetric analysis (TGA) [20] and the optical emission spectroscopy have been used elsewhere [23,24]. However, TGA only gives the sum of the weight gains and weight losses and only provides insights about the chemical evolution of the borosilicate layer. Investigations by emission spectroscopy imply that the chemical species are formed in sufficient quantity in an excited state to be detected through the radiative deactivation process, thus making this technique slightly sensitive. Previously, we have proposed the Laser-Induced Fluorescence (LIF) technique to detect gaseous $BO_2(g)$ radicals above the sample during oxidation of ZrB_2 and ZrB_2-SiC samples [25]. These radical

2

species come from the volatilization of B_2O_3 from the glassy layers. The LIF technique enables the detection of BO_2 radicals with much better sensitivity, spatial and temporal resolutions than emission spectroscopy. Laser excitation of BO_2 is performed at 547.3 nm to promote the $A^2\Pi_u$ (0,0,0) - $X^2\Pi_g$ (0,0,0) vibronic band originating from the ground state. The subsequent fluorescence is detected via the $A^2\Pi_u$ (0,0,0)$\rightarrow X^2\Pi_g$ (1,0,0) red-shifted band at 580 nm [25]. In contrast to the TGA analysis, oxidation detection is delayed since B_2O_3 has to be formed prior to the detection of BO_2(g) [23]. However, the further evolutions of the glassy layer are markedly detected using the LIF technique such as the onset of the oxidation of SiC or the intense volatilization of the glassy layer at temperatures higher than 1500 K.

This paper presents a comparison of the oxidation mechanisms of ZrB_2-SiC, HfB_2-SiC and HfB_2-SiC-Y_2O_3 by using the same real-time LIF detection strategy of evaporated BO_2 above the ZrB_2, ZrB_2-SiC samples heated in air, a technique which has been applied for the first time in our previous article [25]. The influence of the composition on the oxidation behaviour is described in details and the potential of the LIF technique for thermal oxidation detection is confirmed here in the case of the HfB_2-based ceramics.

2. Materials and apparatus

2.1. Materials

Three UHTC compositions are studied: ZrB_2 + 20 vol% SiC, labelled ZS, HfB_2 + 20 vol% SiC, labelled HS and HfB_2 + 20 vol% SiC + 3vol% Y_2O_3, labelled HSY. Properties of the starting powders are listed in Table 1.

Powder	Provider	Grade	d_{50} (µm)	Purity
ZrB_2	H.C. Starck	A	2.8	>97.8
HfB_2	H.C. Starck	A	7.6	>97
SiC	H.C. Starck	BF12	0.6	>98.5
Y_2O_3	Ampere Industrie	-	<5	99.99

Table 1: Grade, purity and particle size of starting powders.

3

After weighing, the powders are attrition-milled in cyclohexane using zirconia media (for ZS) or WC media (for HS and HSY), dried and sieved (50 µm). Fully dense samples (20 to 40 mm in diameter) are obtained using Spark Plasma Sintering (SPS, FCT HD25) in the MATEIS laboratory (Lyon, France). More details concerning manufacturing have already been reported elsewhere [13]. The bulk density and open porosity of these materials are measured by the Archimedes' method. Then, the densification level is calculated as the ratio of the apparent density to the theoretical density of the powder mixture.

Sintering conditions and densification levels of the samples are reported in Table 2.

Composition	Sintering process	Applied pressure	Thermal treatment	Open porosity	Densification rate ρ/ρ_{th}
ZrB_2 + 20 vol% SiC	SPS	28 MPa	2323 K, 2 min	0.1 %	>99 %
HfB_2 + 20 vol% SiC	SPS	16 MPa	2223 K, 5 min	1.8 %	97 %
HfB_2 + 20 vol% SiC + 3vol% Y_2O_3	SPS	7 MPa	2153 K, 5 min	0.1 %	98.5 %

Table 2: Sintering conditions and open porosity of the studied UHTC materials.

2.2. LIF experiment

During the thermal oxidation runs in air of the samples heated with a continuous wave 2 kW CO_2 laser, $BO_2(g)$ is detected in the evaporation plume by monitoring its fluorescence signal at 580 nm induced by laser excitation tuned to 547.3 nm as mentioned above [26]. A very detailed description of the set-up, the method and the experimental protocol were reported in our previous study [25].

The dedicated chamber is equipped with optical windows for laser-based measurements. The CO_2 laser irradiates the target at normal incidence angle from the top of the chamber (figure 1 a). The laser beam is focused on the target in order to irradiate the whole surface. The sample is mounted on an alumina holder in the chamber centre. The support can be translated upwards in order to adjust the height of the sample surface with respect to the probe laser beam axis. Surface temperature is measured with a bichromatic pyrometer in the 1273-2773 K range (Modline 6R-2565, Ircon). Synthetic air (Alphagaz 1) is

injected in the chamber by means of a mass flow regulator, and is evacuated via a pumping system to maintain the pressure constant during the oxidation run.

The probe laser source is a tunable dye laser (Quantel, TDL50) pumped by a pulsed Nd:YAG laser (Quantel, YG781, 10 Hz repletion rate). The pulse duration is 6 ns and the linewidth is 0.07 cm^{-1}. The output energy is 15 mJ/pulse and is attenuated to 1 mJ using neutral density filters. The probe laser beam is crossing the chamber horizontally through anti-reflection coated windows in the visible range. The beam is focused with a spherical lens (f = 600 mm) to obtain a 1 mm laser spot at the sample location in the chamber. During a thermal oxidation run, the laser energy is recorded at the chamber exit by a photodetector (PD10, Ophir) in order to monitor the beam attenuation through the evaporation plume (absorption pathway in figure 1 b)

Fluorescence light is collected at right angle from the probe laser beam axis (fluorescence pathway in figure 1 b) by a 100 mm focal-length lens coupled to an optical fibre (1 mm in diameter). The fluorescence is imaged with a magnification of 1 onto a monochromator (Jobin-Yvon, H-20) equipped with a 1 mm wide exit slit (4 nm bandpass centred at 580 nm). The signal is then detected, amplified, time-integrated (34 ns temporal gate) and averaged (over 10 laser shots) by means of a photomultiplier tube (Photonis, XP2017B) and a Boxcar system (SRS, SR250) [25]. A Labview® interface is used to acquire integrated fluorescence signals via an acquisition PCI card (1.25 MHz, 16 bit) at 10 Hz.

2.3. Experimental protocol

Once the sample is positioned on the holder, the chamber is evacuated prior to synthetic air injection with a 1.3 l/min flow rate. The pressure is regulated to 0.1 MPa, then the heating of the sample and the recording of both the LIF signal and the laser transmission can start. The CO_2-laser power is monitored manually, thus allowing to hold temperature steady to perform timely several adjustments and to ensure that the LIF signal is properly monitored [25].

The nature and the thickness of each oxidised layer were identified through *ex situ* examinations in the Scanning Electron Microscope (SEM, DSM 962) and by Energy Dispersive Spectroscopy (EDS) of both the surface and the polished cross-sections of the oxidised materials.

In addition, TGA experiments (SETSYS Evolution 16/18, SETARAM) are carried out to measure the mass variations during oxidation of each composition. Samples ($2 \times 2 \times 4$ mm^3 in size), are slowly heated (2 K/min) from room temperature to 1823 K under a 50 ml/min air flow.

3. Results

The variation of amplitude of LIF and laser transmission signals as a function of time for ZS, HS and HSY samples is shown in figure 2. As for ZS samples [25], four key steps can be identified for HS and HSY samples and are numbered from ① to ④ in figure 2 but with noticeable differences in the amplitude of signal or in the temperature range associated with each step, as compared in Table 3.

Step ① corresponds to the appearance of the LIF signal indicating that a detectable quantity of $BO_2(g)$ has been formed. This gaseous species comes from the volatilization of the $B_2O_3(l)$ glassy layer formed at the surface of the sample (Reactions 1 and 2).

$$MeB_2 + 5/2\ O_2 \rightarrow MeO_2(s) + B_2O_3\ (l) \tag{1}$$

$$B_2O_3(l) \rightarrow B_2O_3(g) \tag{2}$$

where Me = Zr or Hf.

For all samples, weight gains are observed at lower temperature with TGA (1013 K for ZS and 948 K for HS and HSY) as shown in figure 3. Thus, as already observed, a threshold in boria amount and thus in $B_2O_3(g)$ has to be overstepped before the appearance of the LIF signal. At this temperature (<1473 K), SiC is not yet oxidised (figure 2) [3]. Thus, the following steady rise in the LIF signal between steps ① and ② is attributed to the enhanced

6

volatilization of B_2O_3, leading to an increased quantity of $BO_2(g)$. This is confirmed by the slower increase in weight gain as measured by TGA (figure 3).

An inversion of trend is observed at step ②: the LIF signal slowly decreases despite the continuous rise of sample heating, up to step ③, indicating that less $BO_2(g)$ is formed in this temperature range (Table 3). This striking observation is associated with the beginning of the passive oxidation of SiC through reaction 3. Therefore, the enrichment of the glassy phase with silica increases its stability (higher viscosity) compared to the previous boria glassy layer (reaction 4).

$$SiC + 4O_2 \rightarrow SiO_2(s/l) + CO_2(g) \tag{3}$$

$$SiO_2(l) + B_2O_3(l) \rightarrow \{SiO_2:B_2O_3\}(l) \tag{4}$$

Several studies have already shown that a B_2O_3 concentration gradient is formed in the borosilicate glassy layer as preferential evaporation of B_2O_3 is observed at the surface [27–29]. This lower concentration, and thus the lower activity of B_2O_3 at the surface explains the LIF signal decrease [11,23,29]. Passive oxidation of SiC is also detected using TGA, but at a higher temperature.

Sample	Detection of LIF signal (T_1, ①)	Step ② onset (T_2).	Step ③ onset (T_3)
ZS	1263 K	1553 K	1643 K
HS	1223 K	1433 K	1573 K
HSY	1223 K*	1523 K	1588 K

Table 3: Temperatures of the onset of the three key steps T1, T2 and T3. *extrapolated temperature.

Between steps ③ and ④ small bumps in the LIF signal, immediately followed by a decrease in the signal are observed. This is called the "dynamic phase" and can be explained by a power peak which makes the oxide layer less stable. Thus, the B_2O_3-rich glassy layer, where the activity of B_2O_3 is higher, is exposed and, therefore, the volatilization of B_2O_3 is favoured. The glassy layer is thinner and less protective against oxidation, so that the oxidation of the material underneath is favoured and, as a consequence, quickly reforms a

stable borosilicate glassy layer, and the LIF signal decreases. The subsequent signal bumps have the same origin (power peak) and the same consequences. Between each bump, the average intensity of the LIF signal increases as the temperature is continuously increasing. Compared to TGA, between 1300 and 1673 K, the weight gain increases strongly for HSY, and more smoothly for HS. ZS has a different TGA behaviour, especially at 1473 K. Instead of a decrease in the mass gain slope, which is observed for HS and HSY, there is an increase in this slope. This indicates a continuous oxidation of the materials.

Finally, the high intensity LIF signal peak coupled with a dramatic drop in the laser transmission signal is observed in step ④. At that moment, the probe laser beam is strongly attenuated because of the formation of a dense smoke of oxide particles in the plume, and the LIF signal is no longer detected. This step is also triggered by a power peak, but at this high temperature, the volatilization of the glassy layer is very intense, and the active oxidation of SiC is also favoured via the Reaction 5.

$$SiC + O_2(g) \rightarrow SiO(g) + CO(g). \tag{5}$$

The drop in the transmission signal is linked to the catastrophic volatilization of the glassy layer leading to a high amount of B_2O_3 and SiO particles in the atmosphere just above the sample. However, at 1673 K, the mass gain measured by TGA increases noticeably for all the compositions (figure 3), which confirms that the volatilization of the borosilicate glassy phase promotes the oxidation of the material underneath.

These general trends are observed for all compositions. However, some differences are noticeable, such as the temperatures (T1, T2 and T3) of the onset of the three steps ① to ③, the LIF signals between steps ③ and ④ and the LIF and transmission signals at step ④. These differences are discussed in the next section.

8

4. Discussion

4.1. Formation of the boria glassy phase

Considering Table 3, it can be noticed that the temperature at which the LIF signal is first detected (T_1) is slightly higher for ZS than for HS and HSY. Interestingly, weight gain is detected at lower temperatures in the TGA signal (around 1113 K for ZS and around 948 K for HS and HSY) indicating that the LIF signal $BO_2(g)$ is detected once a boria glassy layer is formed at the surface of the sample (figure 3). The later apparition of the B_2O_3 boria glassy phase and thus of the $BO_2(g)$ detection for ZS samples is observed using both experiments. This can be explained considering the volatility diagrams of ZrB_2 and HfB_2 [30,31] and the diagrams of Ellingham (figure 4). It is clearly shown that oxidation of HfB_2 is favoured at a lower temperature than for ZrB_2.

4.2. Formation of the borosilicate layer

The temperature at which the LIF signal stops increasing (T_2) is higher for ZS and HSY than for HS (~100 K in difference). This phenomenon is worth noting since T_2 marks the moment when $SiO_2(l)$ effectively integrates the boria network to form a borosilicate layer, making it more stable and less subject to volatilization. SEM micrographs of the three materials after oxidation are shown in figures 5 and 6.

The oxidised samples all develop a classic 3-layer oxide scale above the bulk material, from top to bottom: a SiO_2-rich glassy layer, a MeO_2 layer (Me = Zr or Hf) and a SiC-depleted MeB_2 layer. The SiC-depleted layer is formed by active oxidation of SiC (reaction 5), and the reaction product $SiO(g)$ can diffuse towards the surface [32]. Once $SiO(g)$ reaches the borosilicate layer, it can react with dissolved $O_2(g)$ to form $SiO_2(l)$, thus participating in the replenishment of the glassy layer [13,33,34] (reaction 6).

$$SiO(g) + \tfrac{1}{2} O_2(g) \rightarrow SiO_2(l) \qquad (6)$$

From the SEM observations, it should be noted that the SiC-depleted layer has a very different relative thickness depending on the nature of the sample. HS sample develops a very thick SiC-depleted HfB_2 layer (~500 µm, 90% of the total oxide scale), HSY develops a thick SiC-depleted HfB_2 layer (~250 µm, 60% of the total oxide scale) and ZS develops a comparatively thin SiC-depleted ZrB_2 layer (~60 µm, 25% of the total oxide scale) [10,29,32], as reported in Table 4.

	SiC-depleted layer (µm)	Glassy phase layer (µm)	Total oxidised layer (µm)
ZS	60	180	240
HS	500	55	555
HSY	250	170	420

Table 4: Thickness of each layer in the oxidised layers for all the tested compositions (average values from 10 measurements).

Moreover, HS develops a very thin HfO_2 layer compared to the SiC-depleted HfB_2 layer or to other compositions. The composition of the glassy layer surface is directly dependent on the different reaction products that replenish it during the oxidation test. $B_2O_3(l)$ only comes from the oxidation of HfB_2 whereas $SiO_2(l)$ only comes from (directly or via active oxidation) the oxidation of SiC. Thus, the borosilicate layer developed by HS will likely be enriched in $SiO_2(l)$ compared to HSY and ZS. This enrichment leads to an early stabilisation of the glassy layer, and that is why step ② happens at a lower temperature for HS. For HSY, step ② happens at 1523 K, closer to the step ② of ZS (1553 K). First, HSY develops a thinner SiC-depleted layer compared to HS: this means that the borosilicate layer is comparatively enriched in B_2O_3, which delays the stabilisation effect provided by SiO_2. Secondly, the glassy phase is able to solubilise Y_2O_3 during its convection to the surface [21,35,36,13]. Thus, the dissolution of Y_2O_3 in the borosilicate glass decreases its viscosity and, therefore, its capability to act as an oxygen diffusion barrier, since a low viscosity favours the diffusion of oxygen through the borosilicate layer. To form a SiC-depleted layer, the oxygen partial

pressure P_{O2} should be low enough to oxidise SiC without oxidising HfB_2 [32,10,37]. If the glassy layer is less protective towards oxygen diffusion, the formation of a SiC-depleted layer is hindered in favour of the oxidation of both SiC and HfB_2. This explains why, when Y_2O_3 is added to a HfB_2-SiC composition, the stabilisation provided by $SiO_2(l)$ is triggered at a higher temperature. Then, comparing ZS and the two other compositions, ZS exhibits the thinnest SiC-depleted layer and the thickest glassy layer, indicating that the glassy layer formed at the top surface of ZS samples is B_2O_3-rich compared to the glassy phases developed by HS and HSY. Thus, the glassy layer of ZS is more permeable towards oxygen, thus promoting the oxidation of both SiC and ZrB_2 (figure 5 a and b). Another aspect that should be taken into consideration is that, at the experiment temperature (T<1900 K), tetragonal-ZrO_2 is a better oxygen conductor than monoclinic-HfO_2 [38,39]. Thus, this point accentuates the fact that the active oxidation of SiC is not favoured in the ZS composition.

4.3. The dynamic phase

The beginning of step ③ always corresponds to a peak in the LIF signal (figure 2) and a strong increase in the weight gain (figure 3). In this temperature range (>1573 K) the volatilization of B_2O_3 becomes very intense [20] and explains the constant increase in the average level of LIF signal observed in figure 2. However, in the present cases, the volatilization of boria is attenuated by the presence of silica in the glassy layer and the composition of the sample induces some differences in the LIF and transmission signals. For HSY, once the dynamic phase has begun, the average level of the LIF signal remains almost constant, despite the continuous increase in temperature. In parallel, the transmission slowly decreases from 1473 to 1823 K. This means that there is a continuous formation of B_2O_3 droplets and, therefore, a steady volatilization of the borosilicate phase. But, the HSY material developed a very thick borosilicate layer containing a large amount of recrystallised HfO_2 particles (figure 6 b). The thickness of the glassy layer explains its resilience, *i.e.* its capacity

12

to recover an average LIF signal level after the power peak. Moreover, Talmy *et al.* [2] have shown that the presence of immiscible phases in a glassy layer could increase its viscosity and, therefore, limit the diffusion of oxygen. During its convection, the B_2O_3-rich glass is able to solubilise Y_2O_3 and HfO_2. When reaching the surface, B_2O_3 preferentially evaporates, so that Y_2O_3 and HfO_2 attain their saturation concentration and precipitate. Therefore, the continuous volatilization of B_2O_3 throughout the oxidation test favours the continuous precipitation of the solubilised components, which, in turn, increases the stability of the glassy layer.

For ZS, during the dynamic phase, the average level of the LIF signal increases after each peak (figure 2). For this sample, the stabilisation provided by SiO_2 is less effective since the glassy layer is B_2O_3-rich, and the volatilization of B_2O_3 is, therefore, thermo-activated throughout the dynamic phase. The laser transmission signal also decreases steadily; consequently, there is a continuous formation of B_2O_3 droplets. Compared to HSY, the LIF signal takes more time to reach the low level after each signal peak (~180 s compared to ~60 s for HSY). This means that a longer time is required for the sample to regenerate a glassy layer with a good stability. This is mostly due to the fact that the glassy layer of the oxidised ZS sample is B_2O_3-rich, which means that it is more subjected to volatilization, and that a larger quantity is required in order to get the same protection, due to the lower viscosity of B_2O_3-rich borosilicate glass. On the contrary, the glassy layer developed by HSY contains relatively more SiO_2, so that it is more stable, and the material developed a thick SiC-depleted layer, which means that the replenishment of the layer is made with a SiO_2-richer glass, explaining why the glassy layer more rapidly attains stability.

The LIF signal behaviour of HS during oxidation is similar to that of ZS. Each LIF signal peak is followed by an increase in the average LIF signal level. But, contrary to the other samples, the laser transmission signal was almost constant throughout the experiment.

The LIF peaks are also very sharp. To explain these observations, it should be remembered that the borosilicate glass formed by HS is likely very SiO_2-rich, since the SiC-depleted zone is 9 times thicker than the HfO_2 layer. The deficiency in B_2O_3 explains that there is no or not enough formation of B_2O_3 droplets and, therefore, the transmission level is unchanged. It can be noticed that the LIF signal peak at 2100 s (1783 K) is accompanied by a short drop in the transmission level, thus meaning that, at this temperature, some B_2O_3 droplets are formed in a short time. As evidenced in figure 5, the borosilicate layer is likely thin and SiO_2-rich during the test. Contrary to the HSY sample, where the height of LIF signal peaks was about a half of the average LIF signal level, the LIF signal peaks observed for HS are much more prominent, and can be ten times higher than the average LIF signal level. Due to the B_2O_3 deficiency and, therefore, the thinness of the HS borosilicate layer, this glassy phase is much more sensitive to a power peak. After the power peak, the borosilicate layer is even thinner, and this triggers the oxidation of the underlying HfB_2, which will refill the borosilicate glass at the surface.

4.4. Intense volatilization of B_2O_3

Step ④ also illustrated some differences in the oxidation behaviour of the different materials. For the ZS sample, the final LIF signal peak was accompanied by a drastic drop in transmission. For the HS material, this step is characterised by a moderate LIF signal peak and a decrease in the transmission signal. And, finally, for HSY, there is a high intensity LIF signal peak, but there is only a small laser transmission decrease (from 0.7 to 0.6).

Regarding ZS sample, the LIF and transmission signals are associated with a catastrophic volatilization of the B_2O_3-rich borosilicate layer. This is confirmed by the final microstructure of the oxidised ZS sample (figure 5 a), where the glassy layer is very thin or non-existent. However, SEM micrographs of the surface of the oxidised ZS sample (figure 6 a and b) clearly show two features: the first is that, despite the thinness of the glassy layer, it still almost covers the whole surface of the sample, and the second is that the glassy layer is

13

filled with recrystallized ZrO_2 (small particles and large dendritic structures). The crystallites in the glassy layer constitute an indirect proof of the intense volatilization of B_2O_3. The fact that the borosilicate layer covers the entire surface reveals the low viscosity of this layer, probably due to its poverty in SiO_2. The step ④ of HSY is also characterised by an intense LIF signal peak, but not a drastic transmission drop. As explained earlier, the thickness of the glassy layer developed by HSY allows the borosilicate glass to be more resilient towards the power peak. Even if the LIF signal of BO_2 increases, there are not enough B_2O_3 droplets formed to drastically lower the laser transmission and, therefore, the volatilization cannot be qualified as catastrophic. This is confirmed by the SEM observations; the glassy layer is thick (figure 5 e and f) and covers the whole surface (figure 6 e and f). As in the case of ZS, the overwhelming presence of crystallites and dendritic structures of Y_2O_3-doped HfO_2 at the surface constitutes an evidence of the constant volatilization of B_2O_3 during the oxidation test. The case of HS is very different. As explained above, the step ④ of HS is not characterised by an intense LIF signal peak. But a closer examination of the transmission signal reveals that there is a very short but intense drop at 2400 s (1833 K). SEM observations of the HS microstructure showed that the glassy layer was thin (figure 5 c and d) and did not cover the whole surface of the sample (figure 6 c and d). The fact that there is simply not enough B_2O_3 in the remaining borosilicate layer to generate enough detectable BO_2 can explain that there is no intense LIF signal at the end. The lack of B_2O_3 means that the viscosity of the borosilicate layer increases, thus, explaining that the glassy layer does not cover the entire surface of the sample.

5. Conclusion

The oxidation behaviours of ZrB_2-SiC, HfB_2-SiC and HfB_2-SiC-Y_2O_3 materials were studied using the real-time LIF detection of evaporated $BO_2(g)$, above the samples heated up to 1873 K in a dry air atmosphere. For each composition, the starting point of the influence of

SiC on the stability of the glassy layer and the catastrophic volatilization of the glassy layer can be precisely determined. Moreover, the influence of the composition on the oxidation behaviour can be understood and described using this technique.

In order to form a stable glassy layer, the B_2O_3/SiO_2 ratio must be finely tuned. If this ratio is too high, as it seems to be the case for ZS, then the glassy layer is not stabilised enough by SiO_2, and the glassy layer will completely volatilize at ~1873 K. If it is too low, for instance for the HS material, then there is not enough "matter" to create a thick glassy layer that will completely cover the surface of the sample. On the contrary, a good compromise is achieved for HSY: this sample is not only able to generate a thick borosilicate layer, but the preferential volatilization of B_2O_3 will trigger the precipitation of HfO_2 particles, that will in turn increase the stability of the glassy layer in the considered temperature range.

As it was already shown, LIF is a promising method, which can be quantitative, to study *in situ,* and thus continuously, the oxidation behaviour of UHTC. Moreover, the influence of the composition and its ability to form a protective layer can be studied and determined. Thus, the interest of the LIF technique in the detection of thermal oxidation is clearly confirmed.

6. Acknowledgements

7. Data availability

The raw/processed data required to reproduce these findings cannot be shared at this time due to legal or ethical reasons.

8. Authors' contributions

V. Guérineau is the PhD student who has manufactured the samples, tested them, performed the *post-test* analyses and written the article. N. Dorval and G. Vilmart are the specialists of the LIF technique and have helped to modify the bench and prepare the experiments. V. Guérineau, N. Dorval and G. Vilmart have performed all the LIF experiments. A. Julian-Jankowiak is the PhD supervisor, she has helped to modify the bench, to analyse the results and to write the paper.

All the authors have read and approved the final version of this article.

9. Bibliography

1. Opila, E., Levine, S. & Lorincz, J. Oxidation of ZrB_2- and HfB_2-based ultra-high temperature ceramics: effect of Ta additions. *J. Mater. Sci.* **39**, 5969–5977 (2004).
2. Talmy, I. G., Zaykoski, J., Opeka, M. M. & Dallek, S. Oxidation of ZrB_2 ceramics modified with SiC and group IV-VI transition metal diborides. *Electrochem. Soc. Proc.* **12**, 144–158 (2001).
3. Williams, P. A., Sakidja, R., Perepezko, J. H. & Ritt, P. Oxidation of ZrB_2–SiC ultra-high temperature composites over a wide range of SiC content. *J. Eur. Ceram. Soc.* **14**, 3875–3883 (2012).
4. Zhang, P., Hu, P., Zhang, X., Han, J. & Meng, S. Processing and characterization of ZrB_2-SiC_W ultra-high temperature ceramics. *J. Alloys Compd.* **472**, 358–362 (2009).
5. Zhang, S. C., Fahrenholtz, W. G. & Hilmas, G. E. Oxidation of ZrB_2 and ZrB_2-SiC ceramics with tungsten additions. High Temperature Corrosion and Materials Chemistry, *Electrochem. Soc. Trans.* **16**, 137–145 (2008).
6. Carney, C. M., Mogilvesky, P. & Parthasarathy, T. A. Oxidation behavior of zirconium diboride silicon carbide produced by the spark plasma sintering method. *J. Am. Ceram. Soc.* **92**, 2046–2052 (2009).
7. Fahrenholtz, W. G. & Hilmas, G. E. Oxidation of ultra-high temperature transition metal diboride ceramics. *Int. Mater. Rev.* **57**, 61–72 (2012).
8. Monteverde, F. The thermal stability in air of hot-pressed diboride matrix composites for uses at ultra-high temperatures. *Corros. Sci.* **47**, 2020–2033 (2005).
9. Carney, C. M. Oxidation resistance of hafnium diboride-silicon carbide from 1400 to 2000 °C. *J. Mater. Sci.* **44**, 5673–5681 (2009).
10. Shugart, K. & Opila, E. SiC depletion in ZrB_2-30 vol% SiC at ultrahigh temperatures. *J. Am. Ceram. Soc.* **98**, 1673–1683 (2015).
11. Shugart, K., Jennings, W. & Opila, E. Initial stages of ZrB_2-30 vol% SiC oxidation at 1500°C. *J. Am. Ceram. Soc.* **97**, 1645–1651 (2014).
12. Hu, P., Guolin, W. & Wang, Z. Oxidation mechanism and resistance of ZrB_2-SiC composites. *Corros. Sci.* **51**, 2724–2732 (2009).
13. Guérineau, V. & Julian-Jankowiak, A. Oxidation mechanisms under water vapour conditions of ZrB_2-SiC and HfB_2-SiC based materials up to 2400°C. *J. Eur. Ceram. Soc.* **38**, 421–432 (2018).
14. Opila, E. J. & Halbig, M. C. Oxidation of ZrB_2-SiC. *Ceram. Eng. Sci. Proc.* **22**, 221–228 (2001).
15. Nguyen, Q. N., Opila, E. J. & Robinson, R. C. Oxidation of ultrahigh temperature ceramics in water vapor. *J. Electrochem. Soc.* **151**, B558–B562 (2004).
16. Alfano, D., Scatteia, L., Monteverde, F., Bêche, E. & Balat-Pichelin, M. Microstructural characterization of ZrB_2–SiC based UHTC tested in the MESOX plasma facility. *J. Eur. Ceram. Soc.* **30**, 2345–2355 (2010).
17. Marschall, J., Pejaković, D.A., Fahrenholtz, W.G., Hilmas, G.E., Panerai, F. & Chazot, O. Temperature jump phenomenon during plasmatron testing of ZrB_2-SiC ultrahigh-temperature ceramics. *J. Thermophys. Heat Transf.* **26**, 559–572 (2012).
18. Carney, C., Paul, A.,Venugopal, S., Parthasarathy, T., Binner, J., Katz, A. & Brown, P. Qualitative analysis of hafnium diboride based ultra high temperature ceramics under oxyacetylene torch testing at temperatures above 2100°C. *J. Eur. Ceram. Soc.* **34**, 1045–1051 (2014).

19. Paul, A., Venugopal, S., Binner, J., Vaidhyanathan, B., Heaton, A.C.J. & Brown, P. UHTC-carbon fibre composites: preparation, oxyacetylene torch testing and characterisation. *J. Eur. Ceram. Soc.* **33**, 423–432 (2013).

20. Tripp, W. C. & Graham, H. C. Thermogravimetric study of the oxidation of ZrB_2 in the temperature range of 800° to 1500°C. *J. Electrochem. Soc.* **118**, 1195–1199 (1971).

21. Opeka, M. M., Talmy, I. G. & Zaykoski, J. A. Oxidation-based materials selection for 2000°C + hypersonic aerosurfaces: Theoretical considerations and historical experience. *J. Mater. Sci.* **39**, 5887–5904 (2004).

22. Li, H., Yao, X.Y., Zhang, Y.L., Li, K.Z., Guo, L.J., & Liu, L. Effect of heat flux on ablation behaviour and mechanism of C/C–ZrB_2–SiC composite under oxyacetylene torch flame. *Corros. Sci.* **74**, 265–270 (2013).

23. Sevast'yanov, V. G., Simonenko, E.P., Gordeev, A.N., Simonenko, N.P., Kolesnikov, A.F., Papynov, E.K., Shichalin, O.O., Avramenko, V.A. & Kuznetsov, N.T. Behavior of a sample of the ceramic material HfB_2-SiC (45 vol %) in the flow of dissociated air and the analysis of the emission spectrum of the boundary layer above its surface. *Russ. J. Inorg. Chem.* **60**, 1360–1373 (2015).

24. Playez, M., Fletcher, D.G., Marschall, J., Fahrenholtz, W.G., Hilmas, G.E. & Zhu, S. Optical emission spectroscopy during plasmatron testing of ZrB_2-SiC ultrahigh-temperature ceramic composites. *J. Thermophys. Heat Transf.* **23**, 279–285 (2009).

25. Guérineau, V., Julian-Jankowiak, A., Vilmart, G. & Dorval, N. In situ study of the oxidation of ZrB_2 and ZrB_2-SiC materials by monitoring the LIF signal of BO_2 radicals. *Corros. Sci.* **148**, 31–38 (2019).

26. Johns, J. W. C. The absorption spectrum of BO_2. *Can. J. Phys.* **39**, 1738–1768 (1961).

27. Karlsdottir, S. N. & Halloran, J. W. Oxidation of ZrB_2–SiC: influence of SiC content on solid and liquid oxide phase formation. *J. Am. Ceram. Soc.* **92**, 481–486 (2009).

28. Karlsdottir, S. N., Halloran, J. W. & Henderson, C. E. Convection patterns in liquid oxide films on ZrB_2-SiC composites oxidized at a high temperature. *J. Am. Ceram. Soc.* **90**, 2863–2867 (2007).

29. Karlsdottir, S. N. & Halloran, J. W. Formation of oxide scales on zirconium diboride–silicon carbide composites during oxidation: relation of subscale recession to liquid oxide flow. *J. Am. Ceram. Soc.* **91**, 3652–3658 (2008).

30. Fahrenholtz, W. G. The ZrB_2 volatility diagram. *J. Am. Ceram. Soc.* **88**, 3509–3512 (2005).

31. Li, H., Zhang, L., Zeng, Q. & Cheng, L. Thermodynamic calculation of HfB_2 volatility diagram. *J. Phase Equilibria Diffus.* **32**, 422–427 (2011).

32. Fahrenholtz, W. G. Thermodynamic analysis of ZrB_2–SiC oxidation: formation of a SiC-depleted region. *J. Am. Ceram. Soc.* **90**, 143–148 (2007).

33. Parthasarathy, T. A., Rapp, R. A., Opeka, M. & Cinibulk, M. K. Modeling oxidation kinetics of SiC-containing refractory diborides. *J. Am. Ceram. Soc.* **95**, 338–349 (2012).

34. Simonenko, E. P., Sevast'yanov, D. V., Simonenko, N. P., Sevast'yanov, V. G. & Kuznetsov, N. T. Promising ultra-high-temperature ceramic materials for aerospace applications. *Russ. J. Inorg. Chem.* **58**, 1669–1693 (2013).

35. Fahrenholtz, W. G., Hilmas, G. E., Talmy, I. G. & Zaykoski, J. A. Refractory diborides of zirconium and hafnium. *J. Am. Ceram. Soc.* **90**, 1347–1364 (2007).

36. Tian, Z., Zhu, Y. & Huang, W. Effect of yttrium oxide on the viscosity and crystallization of borosilicate glass at high temperature. *Adv. Mater. Res.* **750–752**, 974–977 (2013).

37. Opila, E. J., Smialek, J. L., Robinson, R. C., Fox, D. S. & Jacobson, N. S. SiC recession caused by SiO_2 scale volatility under combustion conditions: II, thermodynamics and gaseous-diffusion model. *J. Am. Ceram. Soc.* **82**, 1826–1834 (1999).

38. Trubelja, M. F. & Stubican, V. S. Ionic conductivity of the fluorite-type hafnia–RE_2O_3 solid solutions. *J. Am. Ceram. Soc.* **74**, 2489–2494 (1991).
39. Corman, G. S. & Stubican, V. S. Phase equilibria and ionic conductivity in the system $ZrO_2-Yb_2O_3-Y_2O_3$. *J. Am. Ceram. Soc.* **68**, 174–181 (1985).

Figures captions

Figure 1: (a) a schematic view of the chamber and (b) LIF set-up.

Figure 2: Surface temperature (left axis), normalised LIF and transmission signals (right axis) vs. time of (a) ZrB$_2$-SiC, (b) HfB$_2$-SiC and (c) HfB$_2$-SiC-Y$_2$O$_3$ materials during an oxidation test in dry air under 0.1 MPa. Key steps (numbered 1 to 4) are described in the text.

Figure 3: Mass variation vs. time of HS, ZS and HSY. Temperature ramp is 2 K /min. The TGA is performed under a 50 ml/min flux of air. Inset: a zoom on TGA signals between 800 and 1200 K.

Figure 4: Diagram of Ellingham for Si, Zr and Hf elements.

Figure 5: SEM micrographs of polished cross-sections of oxidised samples: (a, b) ZS, (c, d) HS and (e, f) HSY. The different layers are (1) borosilicate glass, (2) MeO$_2$ (Me= Zr or Hf), (3) SiC-depleted MeB$_2$ and (4) bulk material.

Figure 6: SEM micrographs of the surfaces of oxidised samples: (a, b) ZS, (c, d) HS and (e, f) HSY materials. In grey, the borosilicate layer and in white, zirconia or hafnia inclusions and dendritic structures. (f) Recrystallised HfO$_2$ is omnipresent (in white) as dendrites and crystallites in the borosilicate layer (grey).
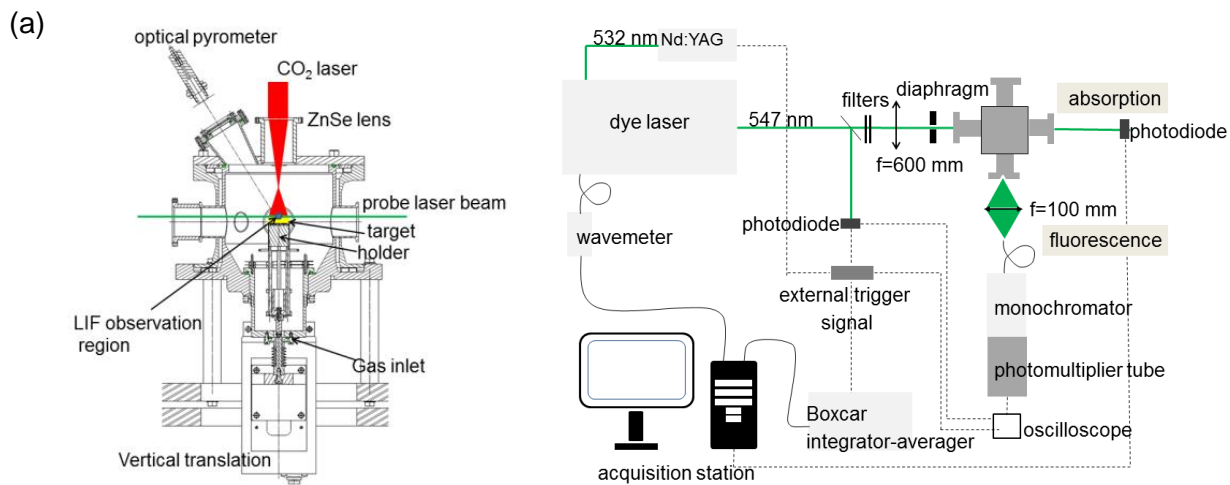
Tables captions:

Table 1: Grade, purity and particle size of starting powders.

Table 2: Sintering conditions and open porosity of the studied UHTC materials.

Table 3: Temperatures of the onset of the three key steps T1, T2 and T3. *extrapolated temperature.

Table 4: Thickness of each layer in the oxidised layers for all the tested compositions (average values from 10 measurements).

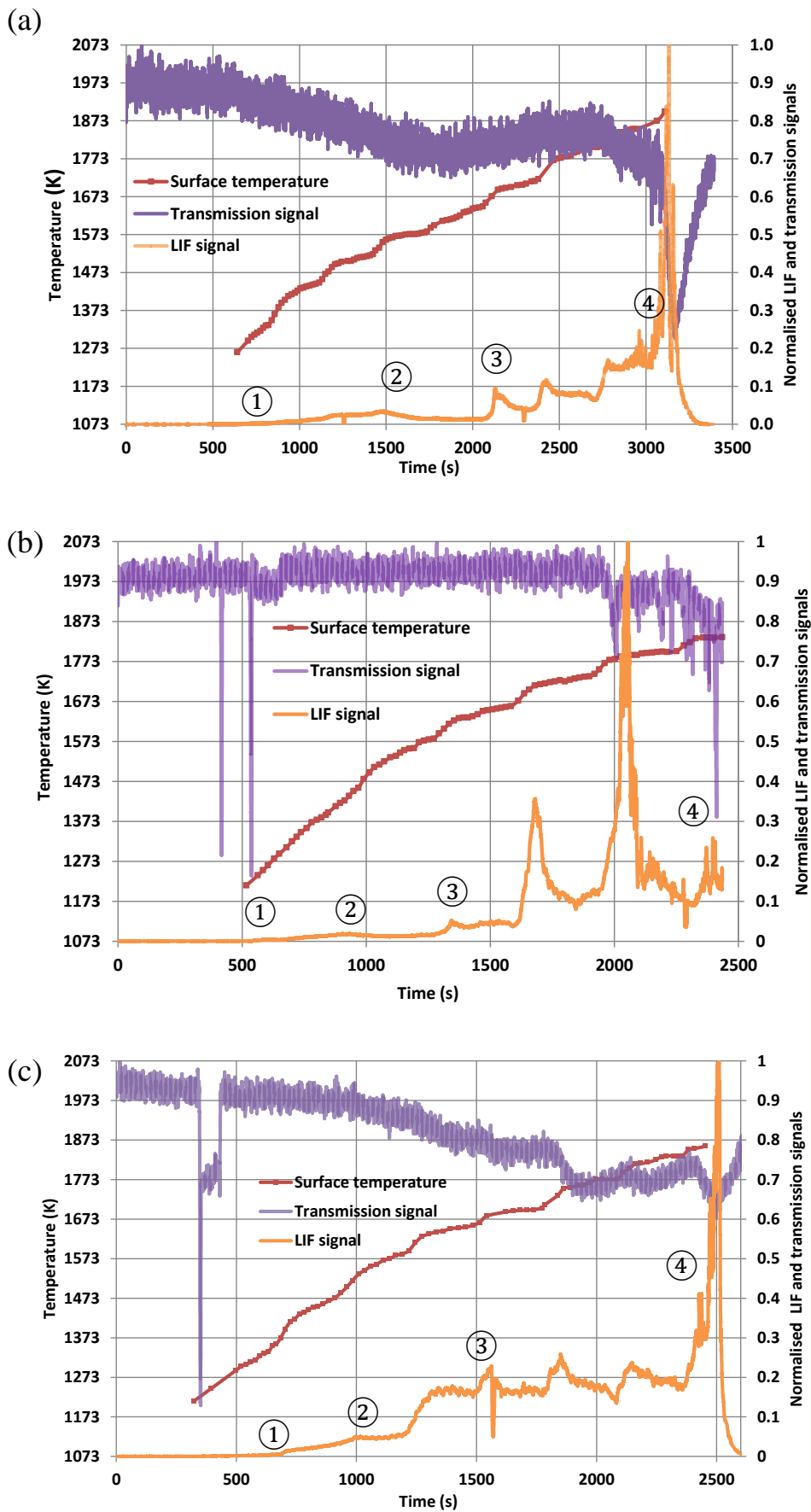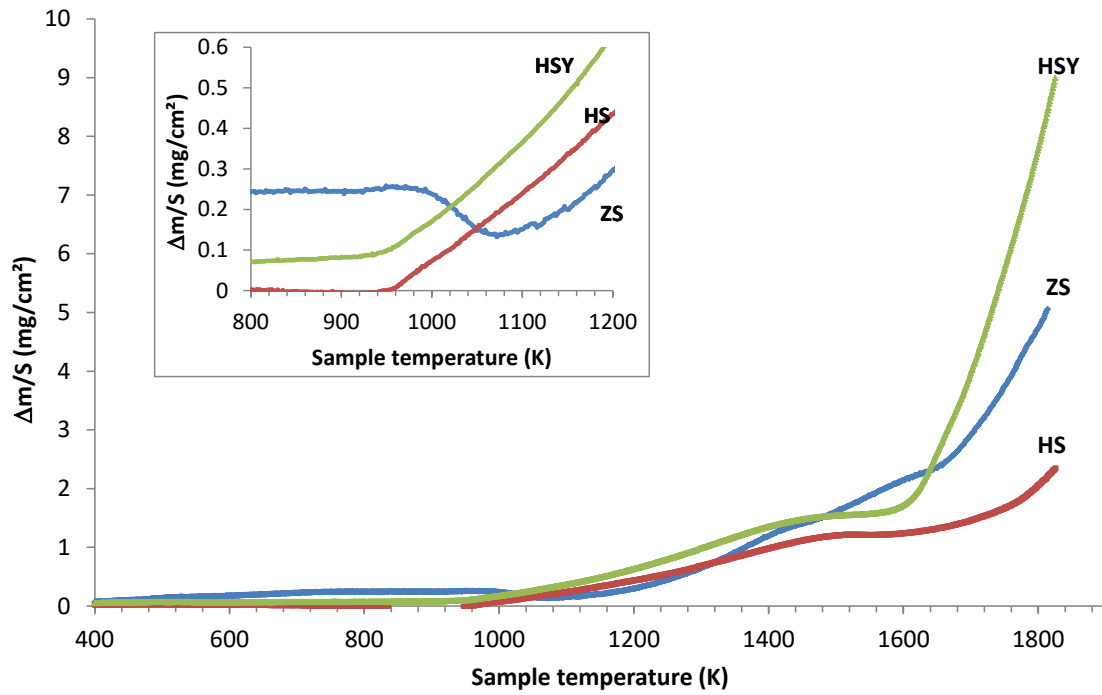**Figure 1: (a) a schematic view of the chamber and (b) LIF set-up.**

Figure 2: Surface temperature (left axis), normalised LIF and transmission signals (right axis) vs. time of (a) ZrB$_2$-SiC, (b) HfB$_2$-SiC and (c) HfB$_2$-SiC-Y$_2$O$_3$ materials during an oxidation test in dry air under 0.1 MPa. Key steps (numbered 1 to 4) are described in the text.

Figure 3: Mass variation vs. time of HS, ZS and HSY. Temperature ramp is 2 K /min. The TGA is performed under a 50 ml/min flux of air. Inset: a zoom on TGA signals between 800 and 1200 K.
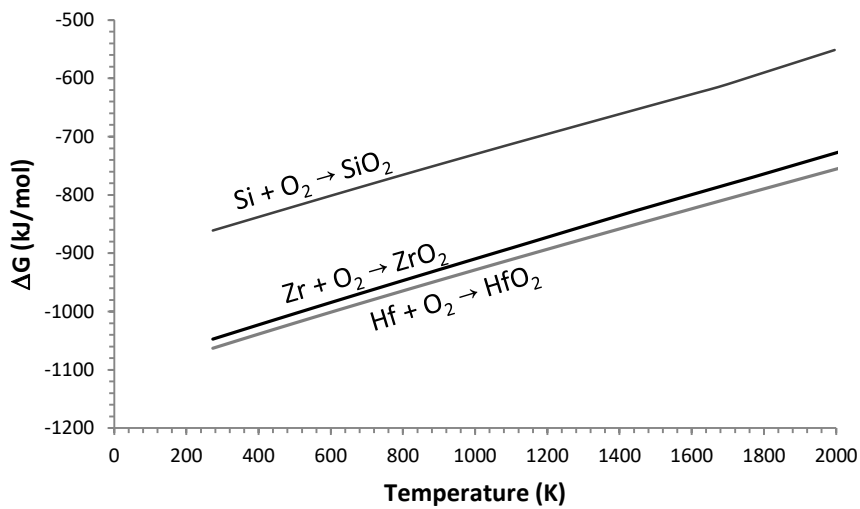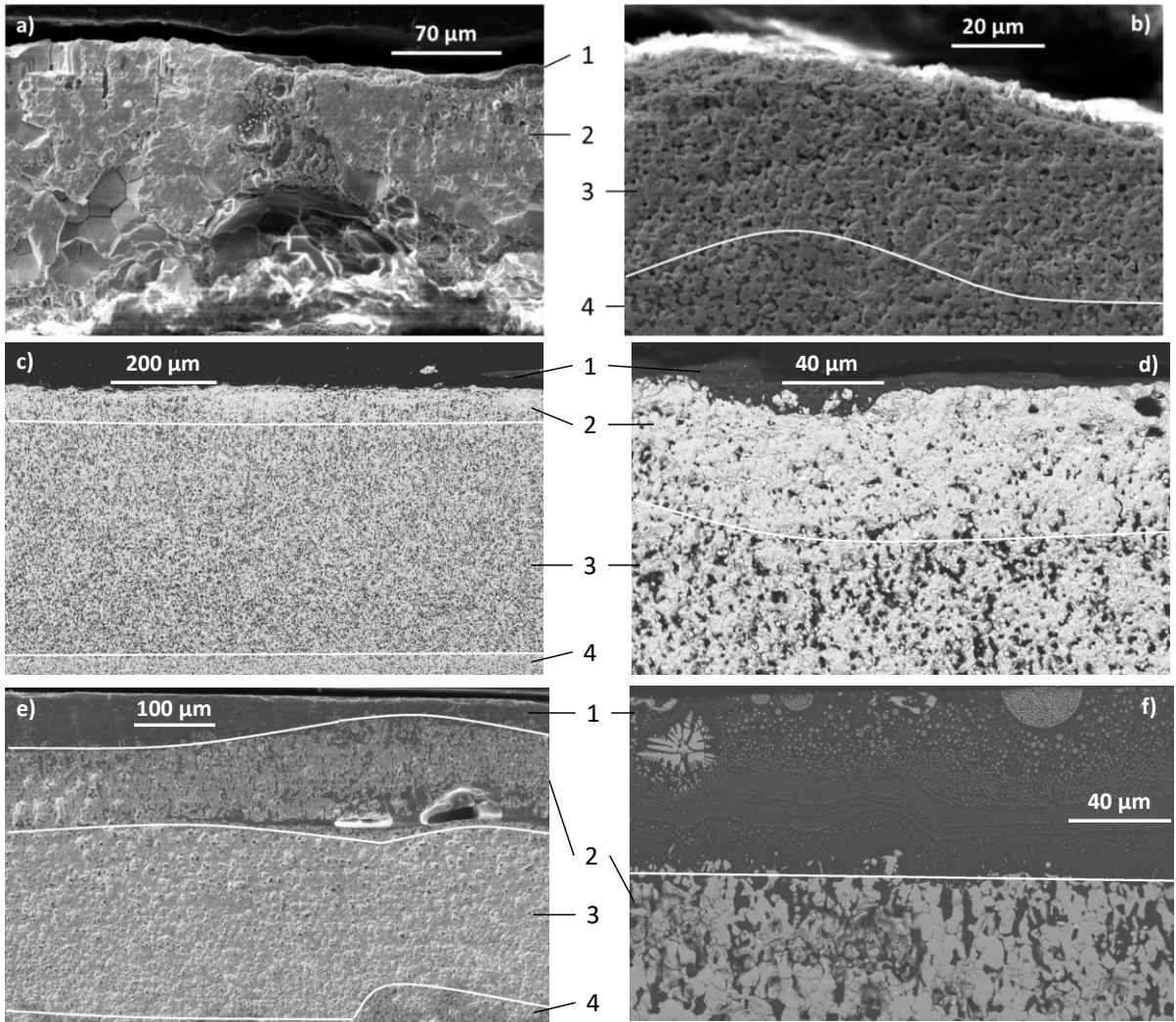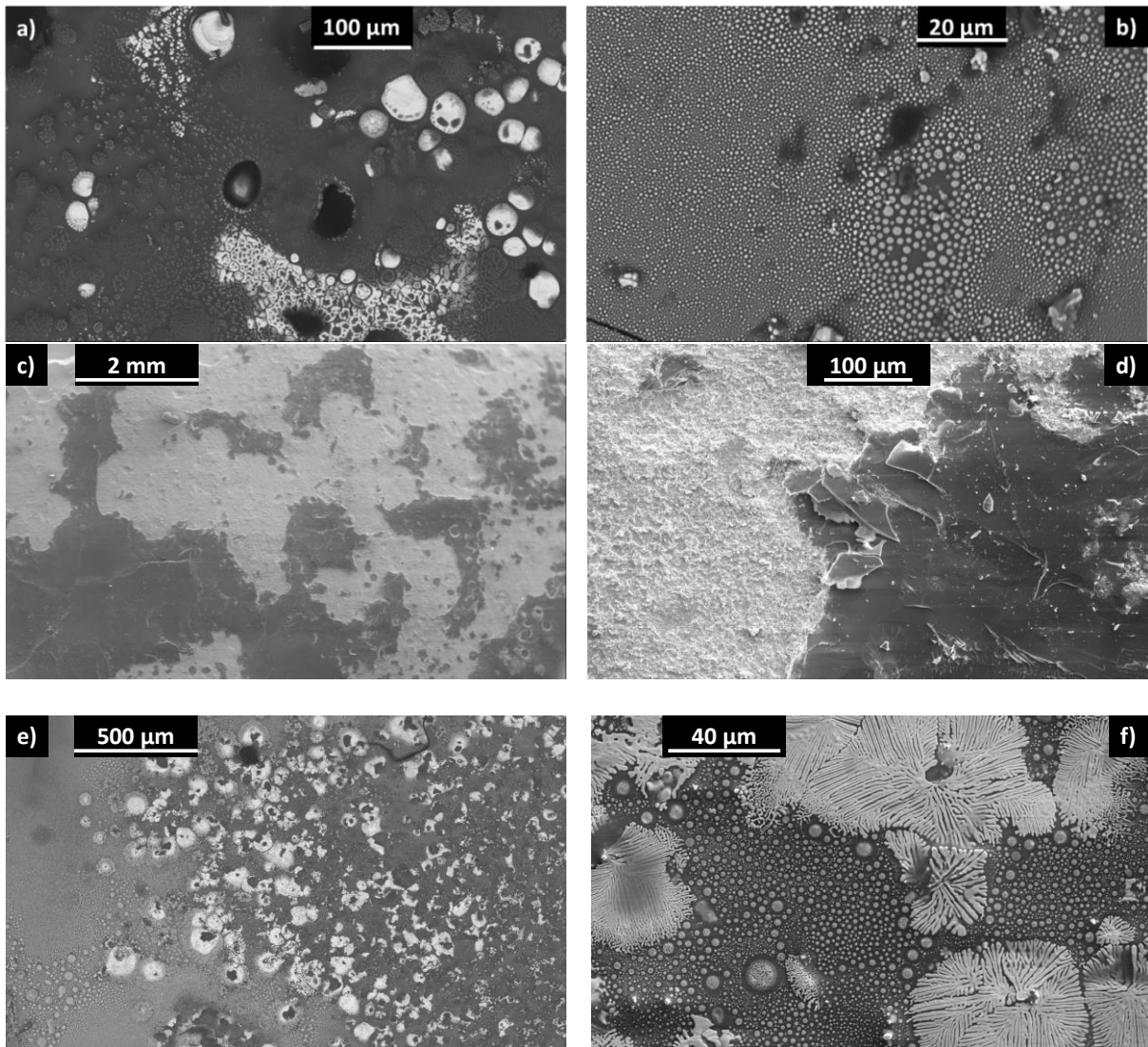

Figure 4: Diagram of Ellingham for Si, Zr and Hf elements.

Figure 5: SEM micrographs of polished cross-sections of oxidised samples: (a, b) ZS, (c, d) HS and (e, f) HSY. The different layers are (1) borosilicate glass, (2) MeO$_2$ (Me= Zr or Hf), (3) SiC-depleted MeB$_2$ and (4) bulk material.

Figure 6: SEM micrographs of the surfaces of oxidised samples: (a, b) ZS, (c, d) HS and (e, f) HSY materials. In grey, the borosilicate layer and in white, zirconia or hafnia inclusions and dendritic structures. (f) Recrystallised HfO_2 is omnipresent (in white) as dendrites and crystallites in the borosilicate layer (grey).